IOP Conf. Series: Journal of Physics: Conf. Series **1270** (2019) 012021 doi:10.1088/1742-6596/1270/1/012021

Experimental and finite element analysis of Cu and Nb severely deformed by 3-axis forging

T Carnrike[1], N Bembridge[2], C Afangideh[3] and P N Kalu[1]

[1] Dept. of Mechanical Engineering, FAMU-FSU College of Engineering, Tallahassee, USA
[2] Formerly at FAMU-FSU College of Engineering, now at Medtronic Inc., MN, USA
[3] Dept. of Mechanical Engineering, Akwa-Ibom State University, Uyo, Nigeria

E-mail: tl12b@my.fsu.edu

Abstract. The evolution of microstructure during 3-Axis Forging (3AF) of OFHC Copper and RRR Niobium has been investigated using both experimental and numerical simulation techniques. The finite element analysis (FEA) aspect was carried out using DEFORM, a commercial software. The 3AF process was conducted at 25°C with a cross-head speed of 0.015 mm s^{-1} and a strain per pass of 0.2. Vickers hardness testing and orientation imaging microscopy (OIM) showed that the evolution of microstructure during 3AF can be classified into three regions: At low strain, region I, in which the high angle grain boundary percentage (HAGB%) declines due to the increase in low angle grain boundary (LAGB) resulting from dynamic recovery. At intermediate strain, region II, there is a progressive increase in HAGB%, due to the conversion of most of the LAGB to high angle grain boundaries (HAGB). This is followed by region III, in which the HAGB% remains relatively unchanged due to a stable microstructure formed by continuous recrystallization. Assessment of the grain size revealed that refinement occurred in regions I and II, resulting in a final grain size of about 2.0 μm and 1.4 μm in Cu and Nb, respectively. Flownet analysis of the first two cycles showed that four deformation zones similar to the hardness pattern were developed in both materials during the 3AF. These zones correlated well with the effective strain and hardness distributions. The highest effective strain and hardness were found in the core of the material (zone A), while the least hardness developed at the edges (zones C and D).

1. Introduction

Severe plastic deformation (SPD) techniques are a group of metal forming procedures, which may be used to impose large strains on materials resulting in significant grain refinement [1]. Some of the SPD techniques include equal channel angular pressing (ECAP), accumulative roll bonding (ARB), high pressure torsion (HPT), and 3-axis forging (3AF) or multi directional forging (MDF). The 3AF process is more attractive because it does not require any special devices, and can be scaled up to be used in industrial applications, in addition to producing nanocrystalline structures [1, 2]. Many studies on the 3AF process have resulted in ultrafine but inhomogeneous microstructures [1]. Wang et al. study on a 2A14 aluminum alloy using 3AF at 450°C utilized a finite element analysis (FEA) flownet approach and experimental techniques. The microstructure was inhomogeneous consisting of four zones [3]. The center (zone I) of the material exhibited the largest effective strain, then the corners (zone II), and finally the top/bottom (zone IV) and side (zone III) edges exhibited the least amount of effective strain [3]. Their study and many others have shown that an experimental approach is not enough to observe

the microstructural evolution throughout the 3AF process thus fueling the need to use FEA. Our work established that the majority of grain refinement of the high purity copper (electronic applications) and niobium (super conducting radio frequency cavities) occurs during the first two cycles of the 3AF process. Therefore, the flownet analysis presented here using DEFORM (FEA software) was confined to the first two cycles and are compared with the results obtained by experimental investigations.

2. Finite Element Analysis

DEFORM-3D, a commercial FEA software was used to investigate 3AF of recrystallized C10100 OFHC copper (99.99%) and Residual Resistively Ratio (RRR) grade Nb (99.99%). The initial dimensions of the billet were 15 mm × 15 mm × 15 mm. The FEA model was constructed using the DEFORM-3D CAD features, in which the sizes of the top and bottom compression plates were as follows: 50.8 mm × 50.8 mm × 9.7 mm. These plates were considered rigid bodies while the billet of material was considered a rigid plastic. The mesh of the billet was generated based on a convergence test which indicated 4,352 8 noded brick elements was sufficient for each model. The process was performed at room temperature (25°C) with a friction coefficient of 0.25 and a strain per pass of 0.2. The analysis of effective strain distribution and flownet was carried out using the DEFORM-3D software for samples deformed to two cycles (cumulative strain of 1.2).

3. Experimental Procedure

The OFHC Cu and Nb samples, as described in the FEA, were subjected to 3AF. The die surfaces (made of hardened D2 tool steel) were finely ground using 3μm diamond solution and multiply coated with colloidal graphite lubricant before each forging pass. The process was carried out at room temperature (25°C) using an MTS hydraulic press at a speed of 0.015 mm s^{-1}. A strain per pass of 0.2 resulting in a 0.6 cumulative strain per cycle was used. The height of the billet of each axis was recorded in order to keep track of the cumulative strain. A total of 16 cycles were completed and this resulted to a cumulative strain of 9.6 and 10 for Cu and Nb, respectively. The samples were prepared, etched and sectioned perpendicular to the second forging axis for proper analysis [4, 5].

Vickers Microhardness Testing (indenter load was 300g), equipped with Computer Assisted Microhardness System (Newage Testing Instruments Inc) and Orientation Imaging Microscopy (OIM) were used for microstructural characterization. The OIM was used in conjunction with Electron Back Scatter Diffraction (EBSD) analysis software package designed by EDAX TSL to interpret the orientation data obtained [6, 7].

4. Results and Discussion

4.1. Orientation imaging microscopy

The starting microstructure of Cu and Nb based on OIM are shown in figures 1 and 2, respectively. The initial grain size (GS), Vickers hardness (HV), and high angle grain boundary percentage (HAGB%) for Cu were 26 μm, 50, and 61 %, respectively. The values for Nb were 134 μm, 50, and 53%, respectively. Upon the completion of the 16 cycles an inhomogeneous microstructure was developed in both materials as can be seen in figures 3 and 4. While the final values of the GS, HV and HAGB% for Cu were 2.0 μm, 116, and 40%, respectively, that of Nb were 1.4 μm, 118, and 59%, respectively. It is evident that the processing resulted in significant grain refinement coupled with hardness increase in both materials. The evolution of HAGB% over the course of processing can be seen in figures 5 and 6 for Cu and Nb, respectively. Three regions can be identified based on the development of HAGB%. Region I occurs at low cumulative strain and is characterized by decreasing HAGB%. Since the actual amount of high angle grain boundaries (HAGB) remains the same as the starting material in this region, it is

reasonable to conclude that there is an increase in the total amount of low angle grain boundaries (LAGB), which leads to the HAGB% in the microstructure to decrease. The increase in the low angle grain boundary percentage (LAGB%) in this region is due to subgrain formation as a result of dynamic recovery [8]. At intermediate cumulative strain, region II, the HAGB% increases due to the conversion of the LAGB to HAGB. Finally, in region III, the structure has become stable, which suggests that discontinuous recrystallization cannot be occurring in this region and as such the microstructure regenerates through continuous recrystallization [8].

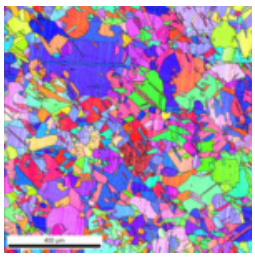

Figure 1. OIM image of the starting Cu material

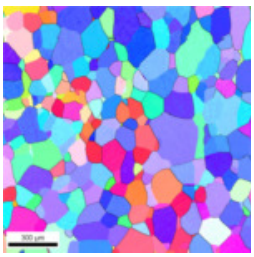

Figure 2. OIM image of the starting Nb material

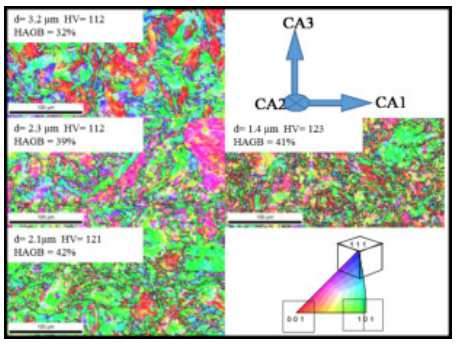

Figure 3. OIM images of the Cu sample after 16 cycles of 3AF at different locations in the sample (top,center,and bottom of left side and core)

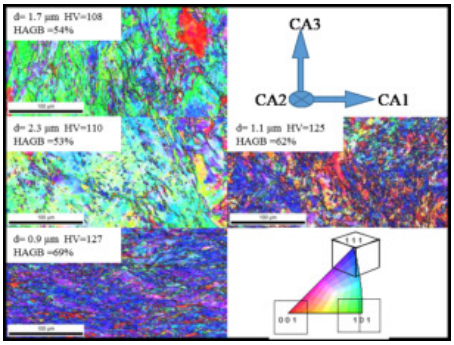

Figure 4. OIM images of the Nb sample after 16 cycles of 3AF at different locations in the sample (top,center,and bottom of left side and core)

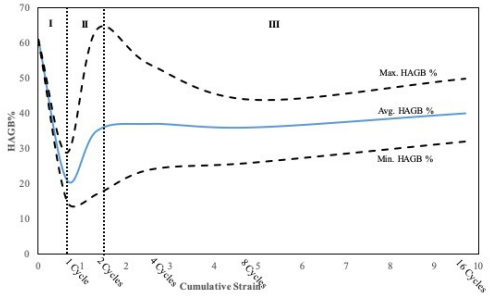

Figure 5. HAGB% of Cu during 3AF

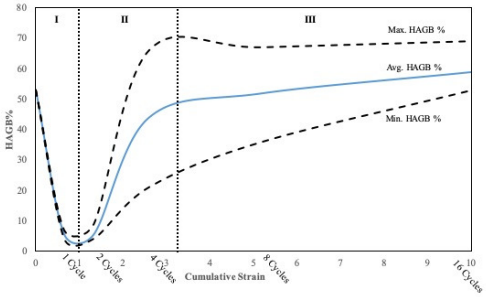

Figure 6. HAGB% of Nb during 3AF

4.2. Effects of 3AF on grain size

Figures 7 and 8 present the assessment of grain refinement in Cu and Nb, respectively. The minimum, maximum, and average GS curves are shown to reflect the inhomogeneity in GS. Superimposing the regions as defined by the HAGB%, it is evident that the grain refinement due to 3AF occurs in regions I and II. Region III is associated with the stabilization of the microstructure.

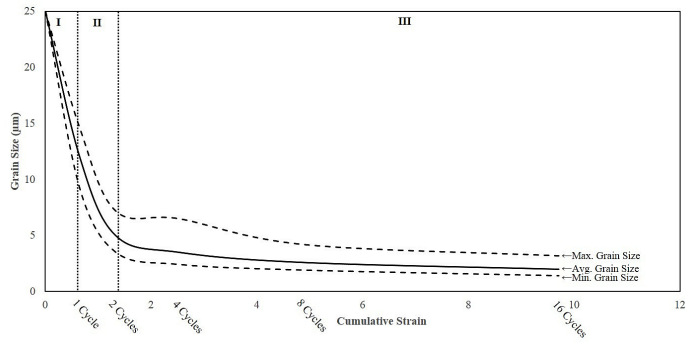

Figure 7. Average GS vs cumulative strain throughout 16 cycles of 3AF for Cu

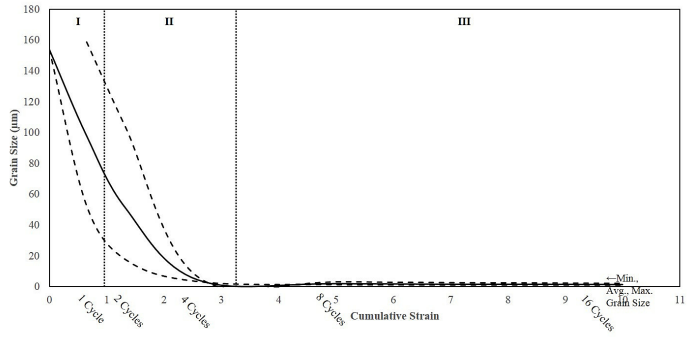

Figure 8. Average GS vs cumulative strain throughout 16 cycles of 3AF for Nb

4.3. Microhardness vs flownet analysis

Figures 9 and 10 show the hardness distributions after 1 cycle in Cu and Nb, respectively. In

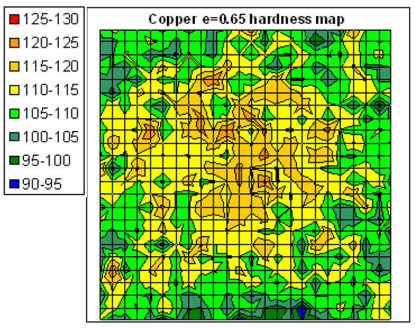

Figure 9. HV distribution after 1 cycle of 3AF for Cu

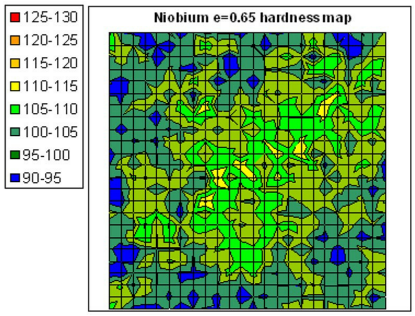

Figure 10. HV distribution after 1 cycle of 3AF for Nb

both cases, the hardness is inhomogeneous. While the highest hardness value was found in the

core (center), the edges exhibited the lowest hardness. After one cycle of 3AF, it is evident that the Cu sample was harder than that of Nb. This means that the Cu sample strain hardened faster than Nb. Unlike the Cu, the niobium sample did not retain its original cubic shape, even after the first cycle. Therefore, there was a need to reshape the Nb after each cycle using a reshaping die. This explains why the hardness distribution shows a higher intensity in a diagonal pattern.

Figure 11 shows the FEA model created and processed using DEFORM software. A flownet analysis for both Cu and Nb has been constructed and that of the first cycle is presented in figures 12 and 13, respectively.

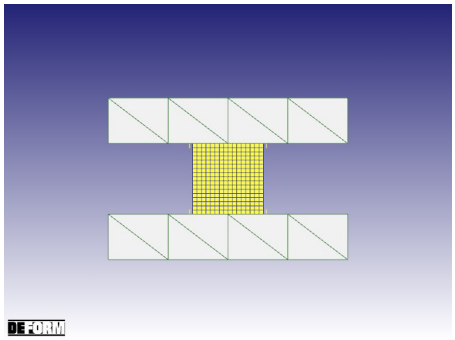

Figure 11. FEA DEFORM 3AF model

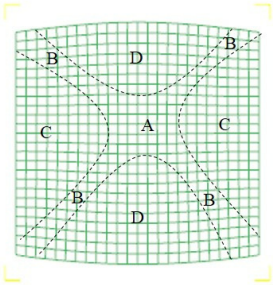

Figure 12. FEA flownet of Cu sample after 1 cycle of 3AF

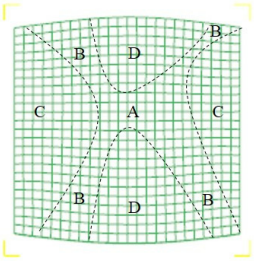

Figure 13. FEA flownet of Nb sample after 1 cycle of 3AF

In both cases four zones were established. These zones were constructed by plotting the flownet at each stage and seeing how it deviates from the starting flownet. The regions with similar flownet deviations were grouped together in a zone. The pattern of the zones in both materials are similar. In zone A, there is little or no deviation of the flownet from the starting flownet. In zone C the flownet protrudes inwards toward zone A while the flownet in zone D protrudes outwards away from zone A. Zone B is a combination of deviation from zones C and D. It is clear that the zones are not symmetrical and this is due to the inhomogeneity in the microstructure as well as the shifting of the billet, from the center of the plates, after each pass. The flownet analysis correlates well with the hardness distributions of figures 9 and 10.

4.4. Effects of cumulative strain on effective strain

Additional analysis of the FEA models was conducted to determine the effective strain distribution. Figures 14 and 15 show the effective strain distribution after the 1st cycle for

Cu and Nb, respectively. The data also prove the existence of the four zones similar to the flownet analysis. A comparison of the flownet analysis and the effective strain distributions clearly correlates the effective strain to hardness. Whereby, high effective strain equates to high hardness, and vice versa. Zone A exhibits the highest effective strain, as it is constantly being put under both tension and compression and is not in contact with the friction from the compression plates. Zone B has the second highest effective strain as it is generally not fully in contact with the compression plates thus the friction effect is not fully present. The smallest effective strain zones are C and D which is due to the presence of friction.

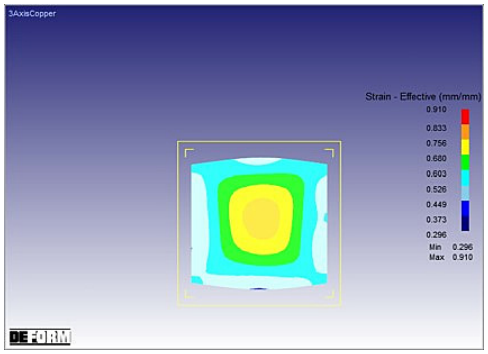

Figure 14. Effective strain distribution of Cu after 1 cycle of 3AF

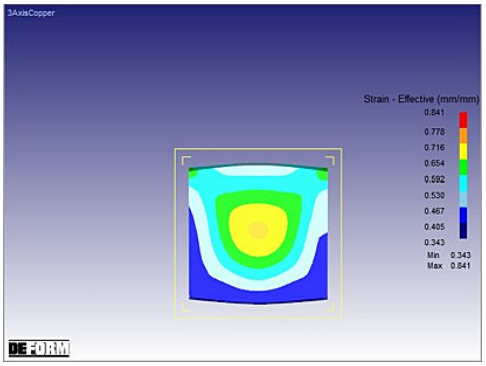

Figure 15. Effective strain distribution of Nb after 1 cycle of 3AF

5. Conclusion

This study used both experimental and FEA techniques to investigate the evolution of microstructure in high purity Cu and Nb subjected to 3AF. Experimental data showed that three regimes of microstructural evolution were present: region I was characterized by subgrain formation due to dynamic recovery. The subgrains were converted to HAGB in region II. The grain structure has been stabilized in region III, suggesting the lack of discontinuous recrystallization. Flownet analysis correlates well with the experimental results and showed that four hardness zones were observed when Cu and Nb were deformed by 3AF. The center (core), zone A, displayed the highest strain and hardness, while zones C and D (edges) had the lowest strain and hardness.

References

[1] Valiev R, Estrin Y, Horita Z, Langdon T, Zechetbauer M and Zhu Y 2006 *J. Miner. Met. Mater. Soc.* Producing Bulk Ultrafine-Grained Materials by Severe Plastic Deformation **58** 33-9
[2] Sitdikov O, Sakai T, Goloborodko A, Miura H and Kaibyshev R 2004 *Mater. Trans.* Effect of Pass Strain on Grain Refinement in 7475 Al Alloy during Hot Multidirectional Forging **45** 2232-8
[3] Wang M, Wang J, Liu W, Ma Y, Liu D, Guo L, Huang L and Huang B 2017 *Int. j. eng. res. eng. sci.* Experimental and Finite Element Analysis of Flow Behavior of 2A14 Aluminum Alloy during Multi-directional Forging **3** 23-32
[4] Bembridge N 2011 *Innovative Severe Plastic Deformation of Niobium with Application to Superconducting Radio Frequency Cavities* dissertation
[5] Vander Voort G 2010 *Metallography, principles and practice* (Materials Park - ASM International)
[6] Adams B, Wright S and Kunze K 1993 *Metall. Mater. Trans. A* Orientation Imaging: The Emergence of a New Microscopy **24A** 819-31
[7] Dingley D 2004 *J. Microsc.* Progressive steps in the development of electron backscatter diffraction and orientation imaging microscopy **213** 214-24
[8] Humphreys F J and Hatherly M 2004 *Recrysallization and Related Annealing Phenomena* edition 2 (Oxford: Elsevier) pp 187,453-5